The far extracellular CUB domain of the adhesion GPCR ADGRG6/GPR126 is a key regulator of receptor signaling

[1]Ethan Dintzner*, [1]Sumit J. Bandekar*, [1]Katherine Leon, [2]Kristina Cechova, [2]Reza Vafabakhsh, and [1]Demet Araç[†]

[1]Department of Biochemistry and Molecular Biology, University of Chicago Neuroscience Institute, Institute for Biophysical Dynamics, and Center for Mechanical Excitability, University of Chicago, Chicago, IL, 60637, USA

[2]Department of Molecular Biosciences, Northwestern University, Evanston, IL, 60208, USA

*These authors contributed equally to this work.

[†]To whom correspondence should be addressed, arac@uchicago.edu

Short Title: Regulation of ADGRG6 by its CUB domain

Keywords: adhesion GPCR, molecular dynamics, ADGRG6, cell signaling, extracellular region

Abstract

Adhesion G Protein–coupled receptors (aGPCRs) transduce extracellular adhesion signals into cytoplasmic signaling pathways. ADGRG6/GPR126 is an aGPCR critical for axon myelination, heart development and ear development; and is associated with developmental diseases and cancers. ADGRG6 has a large, alternatively-spliced, five-domain extracellular region (ECR) that samples different conformations and regulates receptor signaling. However, the molecular details of how the ECR regulates signaling are unclear. Herein, we studied the conformational dynamics of the conserved CUB domain which is located at the distal N-terminus of the ECR and is deleted in an alternatively-spliced isoform (**Δ**CUB). We showed that the **Δ**CUB isoform has decreased signaling. Molecular dynamics simulations suggest that the CUB domain is involved in interdomain contacts to maintain a compact ECR conformation. A cancer-associated CUB domain mutant, C94Y, drastically perturbs the ECR conformation and results in elevated signaling, whereas another CUB mutant, Y96A, located near a conserved Ca^{2+}-binding site, decreases signaling. Our results suggest an ECR-mediated mechanism for ADGRG6 regulation in which the CUB domain instructs conformational changes within the ECR to regulate receptor signaling.

Introduction

Multicellular organisms employ cell–surface receptors to coordinate the intercellular events that are necessary for developmental and regulatory processes. Adhesion G protein–coupled receptors (aGPCRs) represent a diverse and understudied family of cell–surface receptors that couple cellular adhesion to signaling (Lala and Hall, 2022). aGPCRs have critical roles in synapse formation, myelination of the nervous system, angiogenesis, neutrophil activation, embryogenesis, and other biological functions (Yona *et al.*, 2008; Hamann *et al.*, 2015; Langenhan, Piao and Monk, 2016; Lala and Hall, 2022). Additionally, aGPCRs are strongly implicated in developmental diseases, neurological diseases, and cancer (Bassilana, Nash and Ludwig, 2019; Bondarev *et al.*, 2020; Lala and Hall, 2022). Despite their myriad of functions and roles in disease, the molecular mechanisms underlying the function of many aGPCRs remain poorly understood.

aGPCRs contain characteristically large and complex extracellular regions (ECRs) with adhesion domains that bind to ligands (Paavola *et al.*, 2011; Kishore *et al.*, 2016; Salzman *et al.*, 2016, 2017; J. Li *et al.*, 2020; Leon *et al.*, 2020; T. Li *et al.*, 2020; Kordon *et al.*, 2023). The ECR contains a conserved GPCR Autoproteolysis INducing (GAIN) domain which is autoproteolyzed in many aGPCRs. According to the tethered agonist (TA) model of aGPCR activation, removal of the ECR from the membrane-bound seven-pass transmembrane (7TM) region reveals a TA peptide which then activates the receptor (Araç *et al.*, 2012; Lala and Hall, 2022). A large pool of evidence shows that the ECR can also directly modulate 7TM signaling in a TA-independent manner (Kishore *et al.*, 2016; Salzman *et al.*, 2017; Leon *et al.*, 2020; Lala and Hall, 2022; Bui *et al.*, 2023; Bandekar *et al.*, 2024; Kordon *et al.*, 2024). In this second model, communication between ECR and the 7TM is important for the regulation of receptor activity (Lala and Hall, 2022; Kordon *et al.*, 2024). ECR conformation can be affected through the binding of a ligand or by alternative splicing (Araç and Leon, 2019; Leon *et al.*, 2020) and these events are communicated to the 7TM to alter signaling (Kordon *et al.*, 2024). In further support of this idea, roughly half of aGPCRs lack TA-dependent signaling (Dates *et al.*, 2024).

For many aGPCRs, the mechanistic basis by which ECR conformation regulates receptor activity is incompletely understood.

ADGRG6/GPR126 is an evolutionarily conserved aGPCR critical for peripheral nervous system (PNS) myelination, skeletal development, angiogenesis, and heart development (Monk *et al.*, 2011; Patra *et al.*, 2013; Cui *et al.*, 2014; Patra, Monk and Engel, 2014; Sun *et al.*, 2020). The defining characteristic of ADGRG6 is a large 100 kiloDalton (kDa) ECR consisting of the Complement C1r/C1s, Uegf, and Bmp1 (CUB), Pentraxin (PTX), sperm protein, enterokinase and agrin (SEA), Hormone Receptor (HormR), and GAIN domains (Fig. 1A) (Leon *et al.*, 2020). During PNS myelination, the ECR of ADGRG6 is necessary for axon sorting (Monk *et al.*, 2009; Mogha *et al.*, 2013; Petersen *et al.*, 2015). Furthermore, the ECR of ADGRG6 is required for its function in heart development (Patra *et al.*, 2013). Mutations in the ADGRG6 ECR result in loss of PNS myelination and are causative in arthrogryposis multiplex congenita (AMC) (Ravenscroft *et al.*, 2015). Mutations in ADGRG6 could contribute to adolescent idiopathic scoliosis (AIS) disease progression through the ECR (Xu *et al.*, 2019; Leon *et al.*, 2020). Downstream of the receptor, the roles of ADGRG6 in development have been tied to its ability to initiate signaling through the second messenger cyclic adenosine monophosphate (cAMP) (Monk *et al.*, 2009; Mogha *et al.*, 2013; Petersen *et al.*, 2015).

The conformation of the ADGRG6 ECR is correlated with its downstream signaling level (Leon *et al.*, 2020). Previous work suggested that a series of open–like conformations where the N–terminal CUB domain extends away from the other ECR domains drives a higher level of signaling activity. In contrast, a closed and compact ECR conformation formed by the CUB domain engaging the HormR domain, which was observed in a high–resolution crystal structure, corresponds to a lower signaling level (Leon *et al.*, 2020). These conformations are regulated by alternative splicing, where the inclusion (+ss) of a 23–residue splice insert between the PTX and SEA domains (Fig. 1A) shifts the ECR towards the open–like conformation and higher signaling activity (Leon *et al.*, 2020). The –ss splice variant is predominantly found in the closed conformation and has lower signaling activity. The key

difference between these conformations is the location of the CUB domain relative to other ECR domains (Leon *et al.*, 2020).

The ADGRG6 CUB domain is the most conserved domain in the ECR and occupies the far N–terminal position, thus, it has the potential to reach farthest into the extracellular space and interact with ligands. During zebrafish development, transcripts for alternatively-spliced variants encoding ADGRG6 without its CUB domain (termed ∆CUB herein) are detectable (Fig. 1A) (Patra *et al.*, 2013), suggesting that the CUB domain plays an important regulatory role during development. The most conserved portion of the ADGRG6 CUB domain is a Ca^{2+} binding site coordinating a Ca^{2+} ion. The Ca^{2+} binding site on ADGRL6 is a putative ligand binding site, because the same surface is used by other CUB domains to bind extracellular ligands (Gaboriaud *et al.*, 2011; Gingras *et al.*, 2011; Girija *et al.*, 2013). In the closed ECR conformation of ADGRG6 observed in its crystal structure (Leon *et al.*, 2020), the CUB domain uses this surface to engage the HormR domain (Fig. 1B,C). Point mutations on and around the Ca^{2+} binding site lead to PNS myelination and ear development defects in zebrafish (Leon *et al.*, 2020). Additionally, the binding of one putative ADGRG6 ligand, Collagen IV, has been localized to the CUB–PTX tandem (Paavola *et al.*, 2014). Taken together, ADGRG6 ECR conformation may regulate signaling activity through a mechanism involving residues on the Ca^{2+} binding site within the CUB domain. However, the molecular details of this process remain unclear, precluding a comprehensive understanding of ADGRG6 regulation.

In this work, we employ a combination of signaling assays and microsecond–length molecular dynamics (MD) simulations to understand the mechanism by which CUB regulates the function of ADGRG6. We find that the ∆CUB splice variant results in lower cAMP signaling. Using MD simulations, we show that the –ss ADGRG6 ECR adopts multiple closed conformations where the CUB Ca^{2+} binding site remains bound to HormR. The cancer associated mutant C94Y, which is on the CUB domain but distal from the Ca^{2+} binding site, displaces the CUB domain from HormR in MD, and has higher signaling activity than the WT receptor. Another cancer–associated mutant, Y96A, located on the Ca^{2+} binding surface, does not adopt the higher

signaling state. These results suggest that exposure of the CUB domain to solvent stimulates ADGRG6 signaling as long as the Ca^{2+} binding surface is not affected.

Results

The ∆CUB splice variant decreases ADGRG6 cAMP signaling

A developmental splice variant of ADGRG6 has been detected (Patra *et al.*, 2013) which lacks the N–terminal CUB domain (∆CUB, Fig. 1A). As several functions of ADGRG6 depend on its capacity to signal through the cAMP second messenger (Monk *et al.*, 2009; Mogha *et al.*, 2013; Petersen *et al.*, 2015), we first assessed the ability of ADGRG6 ∆CUB to elevate intracellular cAMP levels. We employed a cAMP assay using HEK293 cells transiently transfected with zebrafish ADGRG6 (Fig. 1D) (Mogha *et al.*, 2013; Leon *et al.*, 2020). We tested all constructs for expression using flow cytometry against an N–terminal FLAG tag (Fig. 1E, Supplementary Fig. S1) and found that ∆CUB constructs expressed similarly to WT ADGRG6 constructs. Measured cAMP levels were normalized to the expression of each construct (Fig. 1F). As previously shown (Leon *et al.*, 2020), WT +ss ADGRG6 elevates cAMP at a significantly higher level than the –ss receptor (Fig. 1F). However, we observed both –ss and +ss isoforms of ∆CUB exhibited significantly less cAMP elevation than their WT counterparts (Fig. 1F). Furthermore, the splice site-dependent change in signaling observed with WT ADGRG6 was abolished. These results demonstrate that the ∆CUB splice variant likely plays a different developmental role as it has a decreased ability to elevate cAMP, and that the CUB domain is required for the signaling of ADGRG6.

Microsecond–timescale MD simulations of the ADGRG6 –ss ECR show sustained interdomain contacts involving the CUB, PTX, and SEA domains

As the conformational state of the ADGRG6 ECR correlates with signaling (Leon *et al.*, 2020), we sought to understand the conformational dynamics of the ECR. To this end, we performed several one–microsecond all–atom MD simulations initialized from the crystal structure of the –ss ADGRG6 ECR (Supplementary Fig. S2A–D, and Supplementary Video SV1). Throughout these simulations, the ADGRG6 CUB domain remained associated with HormR. However, the observed ECR conformations were noticeably different from the crystal structure (Fig. 2A–B). The CUB domain interacted with the ECR through a robust interface (CUB:ECR) involving HormR and the linker between PTX and SEA domains through several interactions present in

the crystal structure, as well as several previously unobserved contacts (Fig. 2B, Supplementary Fig. S2E). The CUB:ECR interface included both the Ca^{2+} binding site as well as other CUB domain surfaces. We additionally observed the PTX domain docking onto the SEA domain to form previously unobserved interface (PTX:SEA), which remained intact for the remainder of the simulations. To quantify the extent of the CUB:ECR and PTX:SEA interactions, we performed buried surface area (BSA) and hydrogen bond calculations (Fig. 2C, D). Throughout all simulations, the CUB domain buried approximately 1000 $Å^2$ from solvent and formed on average 10 hydrogen bonds with the rest of the ECR. The PTX:SEA interface buries approximately 350 $Å^2$ from solvent and forms on average 3 interdomain hydrogen bonds. These results suggest that the CUB interaction with the ECR is mediated by a robust network of hydrophobic and hydrophilic contacts involving both the Ca^{2+} binding site and other CUB surfaces, and that the PTX domain could associate with the SEA domain in solution.

ADGRG6 –ss adopts multiple conformations which are distinct from the crystal structure and involve large conformational changes of the CUB–PTX tandem

To quantify ADGRG6 ECR conformational dynamics, we performed principal component analysis (PCA) on our simulations. PCA simplifies the complex conformational landscape observed in our simulations into concerted motions called principal components (PCs). PCA identified two PCs which capture 85% of the conformational variance of our system (Fig. S2F–I). The first of these two PCs describes a ~40º bend of the CUB, PTX, SEA, and HormR domains about the GAIN domain with the CUB–PTX tandem contributing the most inertia (Fig. 3A and Supplementary Video SV2). The second PC is represented by an orthogonal ~60 º bending motion of CUB, PTX, SEA, and HormR domains about the GAIN domain with similar deviation of all domains from the average structure (Fig. 3B and Supplementary Video SV3). During the simulations, a variety of regions in PC space are sampled, highlighting that ADGRG6 can adopt several conformations (Fig. 3C). Hierarchical clusters were generated to classify the projected simulations, revealing clusters whose centroids are distinct conformations from the crystal structure (Fig. 3D) with Cα RMSDs of 13.3 Å, 15.9 Å, and 11.5

Å for centroids 1, 2, and 3 respectively. These data show that the ADGRG6 –ss ECR adopts several conformational states largely through motions of the CUB–PTX tandem, but throughout all these states the CUB domain—including its Ca^{2+} binding site—remains docked to its binding site on HormR.

A cancer-associated CUB mutation, C94Y, breaks the CUB:ECR interface and exposes the Ca^{2+} binding site

The ADGRG6 CUB domain mediates the closed ECR conformation through an extensive contact interface involving not only the Ca^{2+} binding site, but also many distal residues. To investigate the effect of point mutations on the closed conformation, we simulated the C94Y mutant which is present in cancer patients (Cerami *et al.*, 2012). C94Y breaks a disulfide bond between C94 and C111 between CUB and HormR in a CUB domain loop distal to the Ca^{2+} binding site. During the C94Y simulation (Fig. 4, Supplementary Fig. S3, and Supplementary Video SV4), the CUB domain shifted away from the HormR domain and ultimately dissociated from the ECR (Fig. 4A). The CUB domain then bound to a lateral face of HormR, leaving the Ca^{2+} binding site exposed to the solvent. This new, open-like, state is favored over the conformation where CUB is docked to HormR ($\Delta G = -2$ kJ/mol) despite involving a profound loss of BSA between CUB and the ECR (Fig. 4B, C). We then performed PCA to visualize C94Y in comparison to WT (Fig. 4D, Supplementary Fig. S3E, and Supplementary Video SV5, SV6). Using hierarchical clustering, we classified the simulations into four regions, one of which is exclusively occupied by C94Y when its CUB domain is dissociated. These results show that the C94Y mutant adopts a favorable open-like conformation unique from the WT ECR where the Ca^{2+} binding site is exposed to solvent.

The cancer-associated CUB mutation, C94Y, increases receptor activity

To understand how our cancer–associated mutant C94Y which induces an open-like conformation may affect ADGRG6 function, we employed the cAMP assay to test ADGRG6 signaling levels (Fig. 5A, B). We also assayed Y96A, a cancer-associated mutation on the Ca^{2+} binding surface which changes the highly conserved tyrosine that participates in ligand binding in several CUB domains (Gaboriaud *et al.*, 2011; Gingras *et al.*, 2011; Girija *et al.*,

2013; Leon *et al.*, 2020). We assessed the expression levels of ADGRG6 mutants with flow cytometry using an antibody directed against the N–terminal FLAG tag (Fig. 5C, Supplementary Fig. S4) and found both mutants express to a similar level as ADGRG6 WT. Similar to seen previously (Leon *et al.*, 2020), the ADGRG6 –ss isoform signals 5–fold over empty vector (EV) and ADGRG6 +ss signals at a 10–fold level over EV, a significantly higher extent than –ss (Fig. 5D). ADGRG6 C94Y was found super active (~ 14–fold), signaling higher than even the WT +ss receptor. Furthermore, there is no significant difference between C94Y –ss and +ss, in contrast to the isoform–dependence of WT ADGRG6 signaling. The Y96A –ss mutant signaled at a level comparable to WT –ss (Fig. 4D). However, Y96A +ss signaling was 5–fold over EV, similar to WT –ss. This decrease in signaling suggests that the event in WT +ss which leads to elevation of cAMP is not possible in Y96A. Taken together with our computational studies, these results suggest that the dissociation of CUB from the HormR domain may activate ADGRG6, but only if residues in the Ca^{2+} binding surface are unaffected.

Discussion

Despite their essential functions in development and their role in disease, aGPCRs remain an understudied subfamily of cell–surface receptors with enormous therapeutic potential (Bassilana, Nash and Ludwig, 2019; Bondarev *et al.*, 2020). Understanding the molecular basis of aGPCR function is an important step towards therapeutic development. Within the aGPCR family, ADGRG6 has gained attention due to its roles in PNS myelination, angiogenesis, heart and skeletal development, as well as its association with developmental diseases and cancers (Monk *et al.*, 2011; Patra *et al.*, 2013; Cui *et al.*, 2014; Patra, Monk and Engel, 2014; Sun *et al.*, 2020). Here, we describe an ECR–dependent mechanism for ADGRG6 regulation that centers around the far N–terminal CUB domain. Our results clarify previous models of ADGRG6 regulation and may guide future therapeutic development.

The far N-terminal CUB domain of ADGRG6 as a key regulator of signaling

Our data show that the CUB domain of ADGRG6 is regulatory for cAMP signaling. The exposure of the CUB domain to the solvent increases receptor signaling, and the residues in the Ca^{2+} binding surface need to be intact for the regulatory role of the CUB domain (Fig. 6 A-C). We demonstrate that the ∆CUB splice variant produces receptors which have decreased cAMP signaling. In this case, CUB cannot bind to any ligand, intramolecular or otherwise (Fig 6A). For WT ADGRG6 –ss, the ECR samples closed conformations with the CUB domain bound to the HormR domain (Fig. 6B), and a moderate level of signaling is observed. We speculate that CUB binding its intramolecular HormR domain stabilizes an ECR conformation which drives this moderate level of signaling. WT +ss and C94Y favor exposure of the Ca^{2+} binding site to solvent but leave the Ca^{2+} binding surface unaffected (Fig 6C), and we observe these versions of the protein in a higher signaling state than WT –ss. We hypothesize that the open-like ECR conformations, such as those observed in our MD simulations of C94Y, transmit a conformational change to the 7TM that drives this higher signaling.

Finally, the Y96A mutation behaves similarly to the previously characterized D134A/F135A mutation (Leon *et al.*, 2020) in our signaling experiments. Neither of these mutants access the higher signaling levels available to WT +ss or C94Y. Both Y96A and D134/F135A are part of

the ADGRG6 Ca^{2+} binding surface and are key to ligand binding in other CUB domain-ligand complexes (Gaboriaud *et al.*, 2011; Gingras *et al.*, 2011; Girija *et al.*, 2013). These results ascribe further importance to the highly conserved Ca^{2+} binding surface on CUB as a regulator of ECR-dependent signaling.

The aGPCR ECR as an allosteric sensor of ligand binding

Our work on ADGRG6 joins a growing body of work which altogether suggests that aGPCRs use N-terminal portions of their ECRs to sense ligand binding or force; these events can then be transmitted by the ECR to the 7TM to alter signaling. ADGRL3 uses its N-terminal lectin and olfactomedin domains to interact with TEN2 and FLRT (Jackson *et al.*, 2015; Lu *et al.*, 2015; del Toro *et al.*, 2020; J. Li *et al.*, 2020) to instruct synapse specificity, and anti-lectin synthetic antibodies (sABs) can modulate signaling (Kordon *et al.*, 2023). Furthermore, for ADGRL3, anti-GAIN sABs which alter the GAIN/7TM relative orientation can affect receptor signaling (Kordon *et al.*, 2024), supporting an allosteric connection between ECR and 7TM in aGPCRs. ADGRG1 directs myelination through the ligand of its N-terminal PLL domain, transglutaminase-2 (Giera *et al.*, 2018; Salzman *et al.*, 2020), and anti-PLL nanobodies can alter signaling (Salzman *et al.*, 2017). ADGRC1/CELSR1 uses its N-terminal cadherin repeats to mediate homophilic adhesion in trans (Stahley *et al.*, 2021; Bandekar *et al.*, 2024), and may use a compact module of several domains to transmit this signal to the 7TM (Bandekar *et al.*, 2024). The N-terminal PTX domain of ADGRG4 is proposed to dimerize and sense shear force which may result in ADGRG4 activation (Kieslich *et al.*, 2023).

In regards to ADGRG6, this receptor interacts with its putative ligand Collagen IV through the CUB–PTX region of its ECR leading to elevation of cAMP signaling levels (Paavola *et al.*, 2014). Furthermore, two alternatively spliced versions of ADGRG6 both modulate the CUB Ca^{2+} binding surface, providing support for its importance as an ADGRG6 regulatory hotspot. The ΔCUB splice variant removes the entire CUB domain (Patra *et al.*, 2013), preventing the Ca^{2+} binding surface from binding to any ligand, and the +ss splice insert leads to increased solvent exposure of the Ca^{2+} binding site (Leon *et al.*, 2020), disrupting the closed conformation, and allowing it to interact with ligands other than HormR.

Since several ADGRG6 ligands are reported in the literature (Paavola *et al.*, 2014; Petersen *et al.*, 2015; Küffer *et al.*, 2016), it is possible that the Ca^{2+} binding surface on CUB interacts with these ligands or others to regulate receptor function. Additionally, it is possible that conformational changes in the ECR upon disruption of the closed conformation yield the higher signaling activity observed for WT +ss or C94Y. Future structural and mechanistic work will clarify how the CUB Ca^{2+} binding surface modulates receptor function, and perhaps generate tool molecules such as antibodies to bind to the CUB domain and modulate ADGRG6 signaling. Such reagents may have the ability to serve as activators or inhibitors of ADGRG6 signaling and will lay the groundwork for therapeutic development.

Materials and methods

Molecular dynamics simulations

Software used for this work including GROMACS (Abraham *et al.*, 2015) was compiled and maintained by SBGrid (Morin *et al.*, 2013). Simulations were initialized from PDB 6V55 (Leon *et al.*, 2020). Atoms missing from the crystal structure were added with Swiss PDB Viewer. N–linked glycosylation and crystal structure waters were removed from the protein. Using GROMACS, the structure was placed in a 4216.9 nm^3 box with periodic boundary conditions such that all protein atoms are at least 13 Å from the boundaries, resulting in a 160 × 160 × 160 Å cube (Supplementary Fig. S2A). The box was solvated with the SPC water model using gmx solvate and Na^+ and Cl^- counterions were added using gmx genion. The resulting model of ADGRG6 was minimized with the leapfrog integrator in step sizes of 0.1 Å until the max force was smaller than 1000 kJ mol^{-1} nm^{-1}.

The system was then subjected to a two–phase equilibration in the NVT and NPT ensembles with protein atoms under harmonic position restraints. A 100 ps NVT equilibration was carried out with step size 2 fs at 300 K with the Berendsen thermostat using a 0.1 ps coupling constant, and solvent velocities were assigned from the Boltzmann distribution. NPT equilibration was also carried out with step size 2 fs for 100 ps, and at 1 atm with Parrinello–Rahman pressure coupling (2.0 ps coupling constant) using velocities from the NVT ensemble. Simulations on the unrestrained protein were run in the NPT ensemble for 1 μs and a 2 fs step size. Long–range electrostatics were computed with PME with a 1.6 Å Fourier spacing and 10 Å cutoff. All simulations were run with the AMBER99SB–ILDN force field. Replicate simulations were each separately solvated, minimized, and equilibrated.

Simulated systems

Genotype	Splice isoform	Simulation Length	Replicates
WT	–ss	1 μs	3
C94Y	–ss	1 μs	1

PC analysis and free energy landscape analysis

Trajectories from the simulations were extracted for protein atoms and output saved for every ten frames. PCs of the Cαs were calculated by concatenating replicate simulation trajectories for each condition using gmx trjcat and diagonalizing the covariate matrix with gmx covar. Trajectories were projected onto PCs using gmx anaeig and were plotted and visualized with a homemade python script. The fractions of variance f captured by PCs were checked to verify that the first two principal components captured most of the variance and verify the quality of the dimensionality reduction by computing

$$f = \frac{\{\lambda_i\}_{1 \le i \le 3N}}{\mathrm{tr}(C)}$$

where $\{\lambda_i\}_{1 \le i \le 3N}$ is the set of $3N$ eigenvalues for N α–carbons, and $\mathrm{tr}(C)$ is the trace of the covariate matrix. For visualization of trajectories over time on PC space, a Gaussian filter with $\sigma = 50$ was applied to PC1 and PC2 components of each simulation's trajectory. Free energy landscapes were obtained by binning the unfiltered projected simulations into 50×50 bins and computing the Gibbs free energy

$$G = RT\ ln \frac{N_{i,j}}{N_{max}}$$

where $N_{i,j}$ is the number of frames in the ith bin of PC1 and j^{th} bin of PC2 and N_{max} is the number of frames in the most occupied bin. Hierarchical clustering of free energy landscape wells was performed by scipy.cluster in a homemade python script using the Ward clustering method to minimize variance in the l^2 norm. Cluster centroids c_i were computed by averaging the PC1 and PC2 coordinates of frames within each cluster

$$c_i = \frac{1}{N_i} \sum_{j \in \text{ cluster } i} (\text{PC1,PC2})_j$$

where N_i is the number of frames in the ith cluster. We chose the frame from the simulations whose PC coordinates are closest by l^2 norm and constructed the 3D structure as a linear combination of PC1 and PC2 using gmx anaeig. For entropy calculations, we used Schlitter's

formula due to the size of the system and emphasis on higher inertia eigenvectors to approximate an upper bound for the protein's entropy as follows

$$S_{\text{system}} \leq S_{\text{ho}} = \frac{k_B \alpha}{exp(\alpha) - 1} - ln(1 - exp(-\alpha))$$

where

$$\alpha = \frac{\hbar\omega}{k_B T}$$

S_{ho} is the entropy of the harmonic oscillator, and ω is the frequency of the harmonic oscillator related to the variance of the system. Entropy calculations were performed with gmx anaeig –entropy. Cumulative entropy plots were calculated at each time t from the covariate matrix for the portion of the simulation $[0, t]$. Subspace overlap between two different simulations with associated sets of eigenvectors $v_1, v_2, \dots, v_{3N}$ and $\boldsymbol{w}_1, \boldsymbol{w}_2, \dots, \boldsymbol{w}_{3N}$ is found by

$$\text{overlap}(v, w) = \frac{1}{3N} \sum_{i=1}^{3N} \sum_{j=1}^{3N} \left(v_i \cdot w_j\right)^2$$

producing overlap$(\boldsymbol{v}, \boldsymbol{w}) \in [0,1]$. Computation of overlap was carried out with gmx anaeig –over.

Cloning

Wild–type and mutant *D. rerio* (zebrafish) ADGRG6 (Leon *et al.*, 2020) (numbered in this manuscript according to Uniprot ID: C6KFA3) constructs were cloned into pCMV5 by annealing three fragments with the Gibson assembly method. All constructs contain residues 41–1185 and include N–terminal FLAG–tags for measuring cell–surface expression levels. pCMV5 backbone was amplified using the following primers: F: 5' – CGTCCACCAGAAAGGAGCAGTGG 3' and R: 5'– GGGAACCGGAGCTGAATGAAGCC – 3'. The first ADGRG6 –ss Y96A fragment was mutated and amplified from full–length ADGRG6 DNA using F: 5' – AGCACAAGGCTGCATGCGTGACCGCGTTGTCGTC – 3' and R: 5' – CCACTGCTCCTTTCTGGTGGACG 3'; the second Y96A fragment was mutated and amplified from full–length ADGRG6 DNA using F: 5' – GGCTTCATTCAGCTCCGGTTCCC – 3' and R: 5' – GACGACAACGCGGTCAGCGATGCAGCCTTGTGCT – 3'. In a similar scheme

to Y96A, the following fragment: primer combinations were utilized to amplify the –ss ADGRG6 C94Y:

Fragment	Forward Primer (5’ to 3’)	Reverse Primer (5’ to 3’)
C94Y, 1	CGAGGAAGCACAAGGCTACATCTATG ACCGCG	CCACTGCTCCTTTCTGGTGGACG
C94Y, 2	GGCTTCATTCAGCTCCGGTTCCC	CGCGGTCATAGATGTAGCCTTGTG CTTCCTCG

The identity of each construct was confirmed with full–plasmid sequencing.

ΔCUB constructs which contain ADGRG6 residues 149–1185 were generated using an inverse PCR scheme. WT ADGRG6 plasmids were subjected to inverse PCR using the following primers: 5’ AAGCTTGTCGTCATCGTCTT 3’ and 5’ GCAGTGACTCTGAGGAACCA 3’. The resulting linear product contained the entire source plasmid except for the CUB domain. This linear product was circularized using Gibson assembly. The identity of constructs were confirmed using Sanger sequencing.

cAMP signaling assay

HEK293 cells (ATCC CRL–1573) were seeded in 6–well plates with Dulbecco’s Modified Eagle Medium (DMEM; Gibco, 11965092) supplemented with 10 % FBS (Sigma–Aldrich, F0926). At 60–70 % confluency, the cells were co–transfected with 0.35 µg Gpr126 DNA, 0.35 µg GloSensor reporter plasmid (Promega, E2301), and 2.8 µL transfection reagent Fugene 6 (Promega, PRE2693). After a 24–h incubation, the transfected cells were detached and seeded (50,000 cells per well) in a white 96–well assay plate. Following another 24–h incubation, the DMEM was replaced with 100 µL Opti–MEM (Gibco, 31985079) and incubated for 30 min. To each well was then added 1 µL GloSensor substrate and 11 µL FBS. Basal–level luminescence measurements were taken after 30 min to allow for equilibration.

Flow cytometry

HEK293T cells were transfected in a 6–well plate with 1 µg ADGRG6 DNA and 3 µL transfection reagent Fugene 6 (Promega, PRE2693) at 60–70% confluency and incubated for 48 h. The cells were detached with citric saline and washed with phosphate–buffered saline

(PBS). The cells were then washed twice with PBS supplemented with 0.1% BSA (Sigma–Aldrich, A3803). The cells were incubated with mouse anti–FLAG primary antibody (1:1000 dilution in PBS + 0.1% BSA; Sigma–Aldrich, F3165) at room temperature for 30 min and washed three times with PBS + 0.1% BSA. The cells were then incubated with donkey anti–mouse Alexa Fluor 488 secondary antibody (1:500 dilution in PBS + 0.1% BSA; Invitrogen) at room temperature for 30 min and washed three times with PBS + 0.1% BSA. Stained cells were resuspended in PBS + 0.1% BSA and at least 5000 data points were collected with a BD Accuri C6 flow cytometer. The resulting data were analyzed using FloJo v10, single HEK293T cells were gated, and median fluorescence intensity in the 488 channel was used.

Statistical Analysis

All statistical analysis for the cAMP signaling assays was performed using GraphPad Prism Version 10. All experiments were performed in at least N=3 independent experiments each with at least five replicates. For statistical comparisons, the one–way ANOVA with Tukey's correction for multiple comparisons test was used. Each condition was statistically compared with every other condition, but only some comparisons are shown for clarity.

Acknowledgements

We thank Dr. Szymon Kordon for valuable discussion and feedback on this work. This work was supported by a National Institutes of Health Grant R35GM148412 (to DA) and a National Institutes of Health Grant F32GM142266 (to SJB). This work was completed in part with resources provided by the University of Chicago Research Computing Center. The content is solely the responsibility of the authors and does not necessarily reflect the official views of the National Institute of General Medical Sciences or the National Institutes of Health.

Author contributions

Conceptualization: ED, SJB, DA, RV, KC

Methodology: ED, SJB, DA

Investigation: ED, SJB, KL

Visualization: ED, SJB

Supervision: DA

Writing—original draft: ED

Writing—review & editing: ED, SJB, DA

References

Abraham, M. J. *et al.* (2015) 'Gromacs: High performance molecular simulations through multi-level parallelism from laptops to supercomputers', *SoftwareX*, 1–2, pp. 19–25. doi: 10.1016/j.softx.2015.06.001.

Araç, D. *et al.* (2012) 'A novel evolutionarily conserved domain of cell-adhesion GPCRs mediates autoproteolysis', *EMBO Journal*, 31(6), pp. 1364–1378. doi: 10.1038/emboj.2012.26.

Araç, D. and Leon, K. (2019) 'Structure, function and therapeutic potential of adhesion GPCRs', *GPCRs: Structure, Function, and Drug Discovery*, pp. 23–41. doi: 10.1016/B978-0-12-816228-6.00002-7.

Bandekar, S. J. *et al.* (2024) 'Structure of the extracellular region of the adhesion GPCR CELSR1 reveals a compact module which regulates G protein-coupling.', *bioRxiv : the preprint server for biology*. doi: 10.1101/2024.01.26.577439.

Bassilana, F., Nash, M. and Ludwig, M. G. (2019) 'Adhesion G protein-coupled receptors: opportunities for drug discovery', *Nature Reviews Drug Discovery*, 18(11), pp. 869–884. doi: 10.1038/s41573-019-0039-y.

Bondarev, A. D. *et al.* (2020) 'Opportunities and challenges for drug discovery in modulating Adhesion G protein-coupled receptor (GPCR) functions', *Expert Opinion on Drug Discovery*, pp. 1–17. doi: 10.1080/17460441.2020.1791075.

Bui, D. L. H. *et al.* (2023) 'The adhesion GPCRs CELSR1-3 and LPHN3 engage G proteins via distinct activation mechanisms.', *Cell reports*, 42(6), p. 112552. doi: 10.1016/j.celrep.2023.112552.

Cerami, E. *et al.* (2012) 'The cBio Cancer Genomics Portal: An open platform for exploring multidimensional cancer genomics data', *Cancer Discovery*, 2(5), pp. 401–404. doi: 10.1158/2159-8290.CD-12-0095.

Cui, H. *et al.* (2014) 'GPR126 protein regulates developmental and pathological angiogenesis through modulation of VEGFR2 receptor signaling', *Journal of Biological Chemistry*, 289(50), pp. 34871–34885. doi: 10.1074/jbc.M114.571000.

Dates, A. N. *et al.* (2024) 'Heterogeneity of tethered agonist signaling in adhesion G protein-coupled receptors', *Cell Chemical Biology*, pp. 1–12. doi: 10.1016/j.chembiol.2024.03.004.

Gaboriaud, C. *et al.* (2011) 'Structure and properties of the Ca 2+ -binding CUB domain, a widespread ligand-recognition unit involved in major biological functions', *Biochemical Journal*, 439(2), pp. 185–193. doi: 10.1042/BJ20111027.

Giera, S. *et al.* (2018) 'Microglial transglutaminase-2 drives myelination and myelin repair via GPR56/ADGRG1 in oligodendrocyte precursor cells', *eLife*, 7, pp. 1–25. doi: 10.7554/eLife.33385.

Gingras, A. R. *et al.* (2011) 'Structural basis of mannan-binding lectin recognition by its associated serine protease MASP-1: Implications for complement activation', *Structure*, 19(11), pp. 1635–1643. doi: 10.1016/j.str.2011.08.014.

Girija, U. V. *et al.* (2013) 'Structural basis of the C1q/C1s interaction and its central role in assembly of the C1 complex of complement activation', *Proceedings of the National Academy of Sciences of the United States of America*, 110(34), pp. 13916–13920. doi: 10.1073/pnas.1311113110.

Hamann, J. *et al.* (2015) 'International union of basic and clinical pharmacology. XCIV. adhesion G protein-coupled receptors', *Pharmacological Reviews*, 67(2), pp. 338–367. doi: 10.1124/pr.114.009647.

Jackson, V. A. *et al.* (2015) 'Structural basis of latrophilin-FLRT interaction', *Structure*, 23(4), pp. 774–781. doi: 10.1016/j.str.2015.01.013.

Kieslich, B. *et al.* (2023) 'The dimerized pentraxin-like domain of the adhesion G protein–coupled receptor 112 (ADGRG4) suggests function in sensing mechanical forces', *Journal of Biological Chemistry*, 299(12), p. 105356. doi: 10.1016/j.jbc.2023.105356.

Kishore, A. *et al.* (2016) 'Stalk-dependent and stalk-independent signaling by the adhesion G protein-coupled receptors GPR56 (ADGRG1) and BAI1 (ADGRB1)', *Journal of Biological Chemistry*, 291(7), pp. 3385–3394. doi: 10.1074/jbc.M115.689349.

Kordon, S. P. *et al.* (2023) 'Isoform- and ligand-specific modulation of the adhesion GPCR ADGRL3/Latrophilin3 by a synthetic binder', *Nature Communications*, 14(1). doi: 10.1038/s41467-023-36312-7.
Kordon, S. P. *et al.* (2024) 'Structural analysis and conformational dynamics of a holo-adhesion GPCR reveal interplay between extracellular and transmembrane domains.', *bioRxiv : the preprint server for biology*. doi: 10.1101/2024.02.25.581807.
Küffer, A. *et al.* (2016) 'The prion protein is an agonistic ligand of the G protein-coupled receptor Adgrg6', *Nature*, 536(7617), pp. 464–468. doi: 10.1038/nature19312.
Lala, T. and Hall, R. A. (2022) 'ADHESION G PROTEIN-COUPLED RECEPTORS: STRUCTURE, SIGNALING, PHYSIOLOGY, AND PATHOPHYSIOLOGY', *Physiological Reviews*. American Physiological Society, pp. 1587–1624. doi: 10.1152/physrev.00027.2021.
Langenhan, T., Piao, X. and Monk, K. R. (2016) 'Adhesion G protein-coupled receptors in nervous system development and disease', *Nature Reviews Neuroscience*, 17(9), pp. 550–561. doi: 10.1038/nrn.2016.86.
Leon, K. *et al.* (2020) 'Structural basis for adhesion G protein-coupled receptor Gpr126 function', *Nature Communications*, 11(1). doi: 10.1038/s41467-019-14040-1.
Li, J. *et al.* (2020) 'Alternative splicing controls teneurin-latrophilin interaction and synapse specificity by a shape-shifting mechanism', *Nature Communications*, 11(1), p. 2140. doi: 10.1038/s41467-020-16029-7.
Li, T. *et al.* (2020) 'A splicing isoform of GPR56 mediates microglial synaptic refinement via phosphatidylserine binding', *The EMBO Journal*, 39(16), pp. 1–20. doi: 10.15252/embj.2019104136.
Lu, Y. C. *et al.* (2015) 'Structural Basis of Latrophilin-FLRT-UNC5 Interaction in Cell Adhesion', *Structure*, 23(9), pp. 1678–1691. doi: 10.1016/j.str.2015.06.024.
Mogha, A. *et al.* (2013) 'Gpr126 functions in schwann cells to control differentiation and myelination via G-protein activation', *Journal of Neuroscience*, 33(46), pp. 17976–17985. doi: 10.1523/JNEUROSCI.1809-13.2013.
Monk, K. R. *et al.* (2009) 'A G protein-coupled receptor is essential for schwann cells to initiate myelination', *Science*, 325(5946), pp. 1402–1405. doi: 10.1126/science.1173474.
Monk, K. R. *et al.* (2011) 'Gpr126 is essential for peripheral nerve development and myelination in mammals', *Development*, 138(13), pp. 2673–2680. doi: 10.1242/dev.062224.
Morin, A. *et al.* (2013) 'Collaboration gets the most out of software', *eLife*, 2013(2), pp. 1–6. doi: 10.7554/eLife.01456.
Paavola, K. J. *et al.* (2011) 'The N terminus of the adhesion G protein-coupled receptor GPR56 controls receptor signaling activity', *Journal of Biological Chemistry*, 286(33), pp. 28914–28921. doi: 10.1074/jbc.M111.247973.
Paavola, K. J. *et al.* (2014) 'Type IV collagen is an activating ligand for the adhesion G protein-coupled receptor GPR126', *Science Signaling*, 7(338), pp. 1–10. doi: 10.1126/scisignal.2005347.
Patra, C. *et al.* (2013) 'Organ-specific function of adhesion G protein-coupled receptor GPR126 is domain-dependent', *Proceedings of the National Academy of Sciences of the United States of America*, 110(42), pp. 16898–16903. doi: 10.1073/pnas.1304837110.
Patra, C., Monk, K. R. and Engel, F. B. (2014) 'The multiple signaling modalities of adhesion G protein-coupled receptor GPR126 in development.', *Receptors & clinical investigation*, 1(3), p. 79. doi: 10.14800/rci.79.
Petersen, S. C. *et al.* (2015) 'The Adhesion GPCR GPR126 Has Distinct, Domain-Dependent Functions in Schwann Cell Development Mediated by Interaction with Laminin-211', *Neuron*, 85(4), pp. 755–769. doi: 10.1016/j.neuron.2014.12.057.
Ravenscroft, G. *et al.* (2015) 'Mutations of GPR126 Are Responsible for Severe Arthrogryposis Multiplex Congenita', *American Journal of Human Genetics*, 96(6), pp. 955–961. doi: 10.1016/j.ajhg.2015.04.014.
Salzman, G. S. *et al.* (2016) 'Structural Basis for Regulation of GPR56/ADGRG1 by Its Alternatively Spliced Extracellular Domains', *Neuron*, 91(6), pp. 1292–1304. doi: 10.1016/j.neuron.2016.08.022.

Salzman, G. S. *et al.* (2017) ‘Stachel-independent modulation of GPR56/ADGRG1 signaling by synthetic ligands directed to its extracellular region’, *Proceedings of the National Academy of Sciences of the United States of America*, 114(38), pp. 10095–10100. doi: 10.1073/pnas.1708810114.
Salzman, G. S. *et al.* (2020) ‘Specific and direct modulation of the interaction between adhesion GPCR GPR56/ADGRG1 and tissue transglutaminase 2 using synthetic ligands’, *Scientific Reports*, 10(1), pp. 1–9. doi: 10.1038/s41598-020-74044-6.
Stahley, S. N. *et al.* (2021) ‘Celsr1 adhesive interactions mediate the asymmetric organization of planar polarity complexes’, *eLife*, 10, pp. 1–26. doi: 10.7554/eLife.62097.
Sun, P. *et al.* (2020) ‘Regulation of body length and bone mass by GPR126/Adgrg6’, *Science Advances*, 6(12), pp. 1–13. doi: 10.1126/sciadv.aaz0368.
del Toro, D. *et al.* (2020) ‘Structural Basis of Teneurin-Latrophilin Interaction in Repulsive Guidance of Migrating Neurons’, *Cell*, 180(2), pp. 323-339.e19. doi: 10.1016/j.cell.2019.12.014.
Xu, E. *et al.* (2019) ‘A Genetic Variant in GPR126 Causing a Decreased Inclusion of Exon 6 Is Associated with Cartilage Development in Adolescent Idiopathic Scoliosis Population’, *BioMed Research International*, 2019(February 2018). doi: 10.1155/2019/4678969.
Yona, S. *et al.* (2008) ‘Adhesion-GPCRs: emerging roles for novel receptors’, *Trends in Biochemical Sciences*, 33(10), pp. 491–500. doi: 10.1016/j.tibs.2008.07.005.

Figures

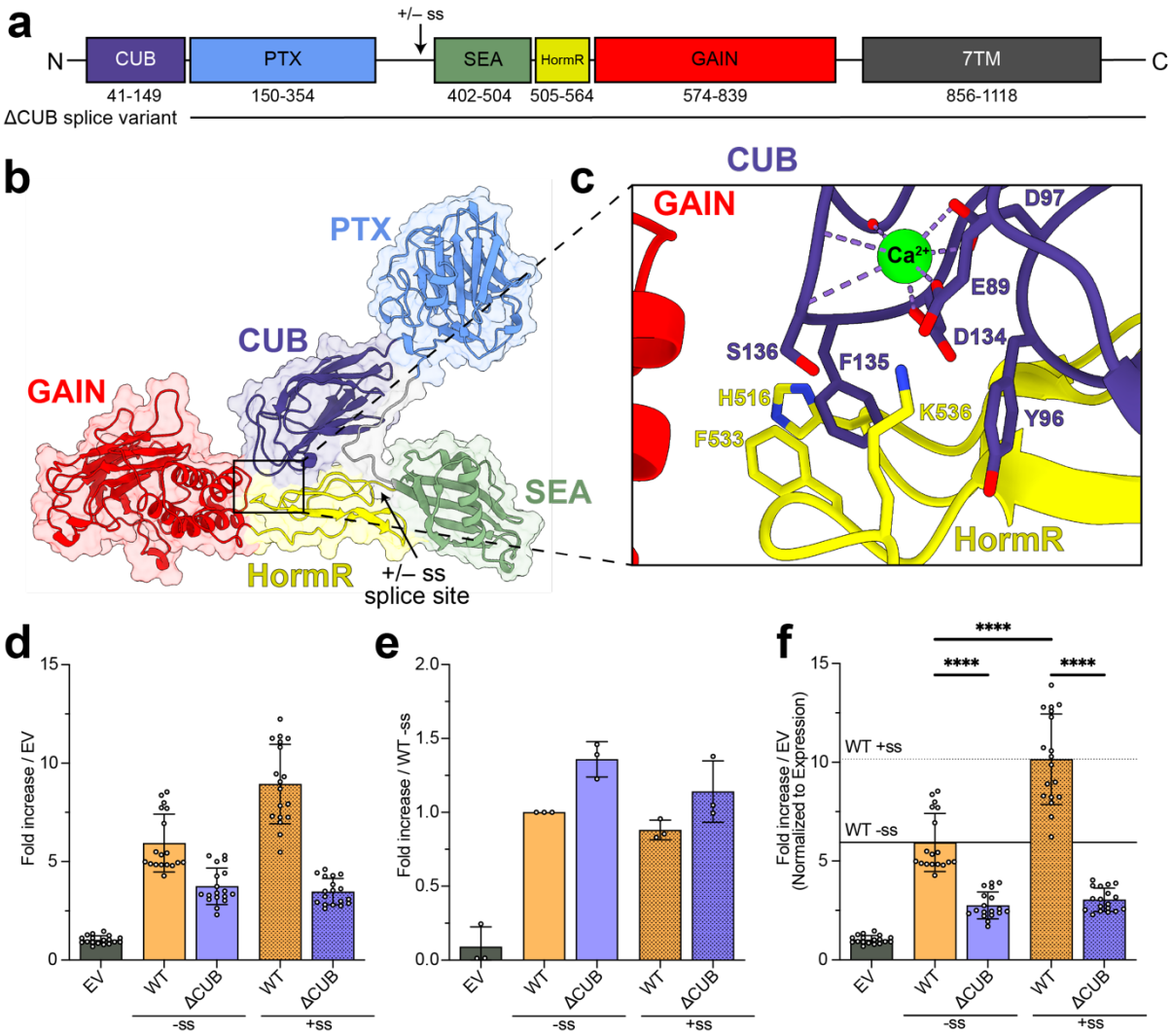

Fig. 1: Deletion of the CUB domain decreases ADGRG6–dependent cAMP signaling. (a): Linear domain diagram for ADGRG6. The ΔCUB splice variant is depicted as a horizontal black line to show its domain boundaries. The position of the splice site between PTX and SEA is designated by an arrow. **(b):** ADGRG6 –ss ECR crystal structure (PDB 6V55) depicted using cartoon along with surface representation. **(c):** Close–up of the CUB/HormR interface from the crystal structure with key residues involved in the interaction shown as sticks. The bound Ca^{2+} ion is shown as a green sphere with coordination shown as dotted lines. **(d):** Basal cAMP signaling of ADGRG6 constructs shown as fold change over empty vector (EV). Mutants are grouped by absence (–ss) or presence (+ss) of the ECR splice insert. **(e):** Relative cell surface expression levels for ADGRG6 constructs shown as fold increase over WT –ss. See Supplementary Fig. S1 for raw flow cytometry data. **(f):** Basal cAMP signaling shown as fold change over empty vector (EV) normalized to cell–surface expression. Mutants are grouped by absence (–ss) or presence (+ss) of the ECR splice insert. Horizontal lines show the mean normalized signaling levels for WT constructs. **** – $p<0.0001$; one–way ANOVA test with Tukey's correction for multiple comparisons. Each condition was compared to every other condition, but not all comparisons are shown for clarity. N=3 independent experiments were performed with six replicates each.

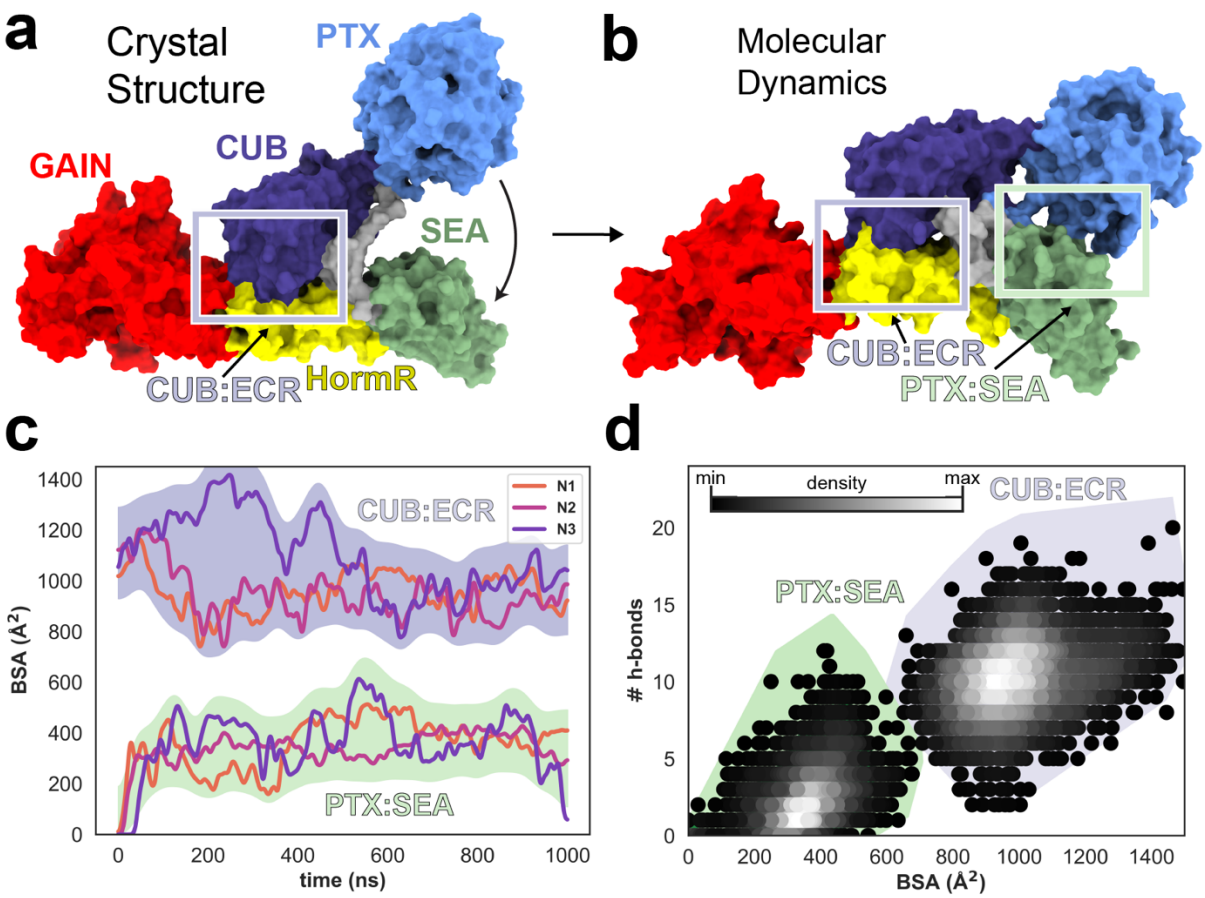

Fig. 2: Molecular dynamics simulations of ADGRG6 –ss show sustained interdomain contacts involving the CUB, PTX, and SEA domains. (a): Surface representation of ADGRG6 from the crystal structure with the CUB:ECR interface shown as a light purple rectangle. **(b):** A representative frame from the MD simulations showing the conformational differences. The CUB:ECR and PTX:SEA interfaces are shown as light purple and light green rectangles, respectively. **(c):** Buried surface area (BSA) of CUB:ECR and PTX:SEA interfaces plotted over simulation time. Colored lines show each individual simulation, and the shaded areas represent the upper and lower bounds of all simulations. **(d):** The number of hydrogen bonds plotted versus the BSA of the described interfaces. The density (% of frames) of each position is plotted as a series of circles, with the most occupied regions of the plot in white, and the least in black.

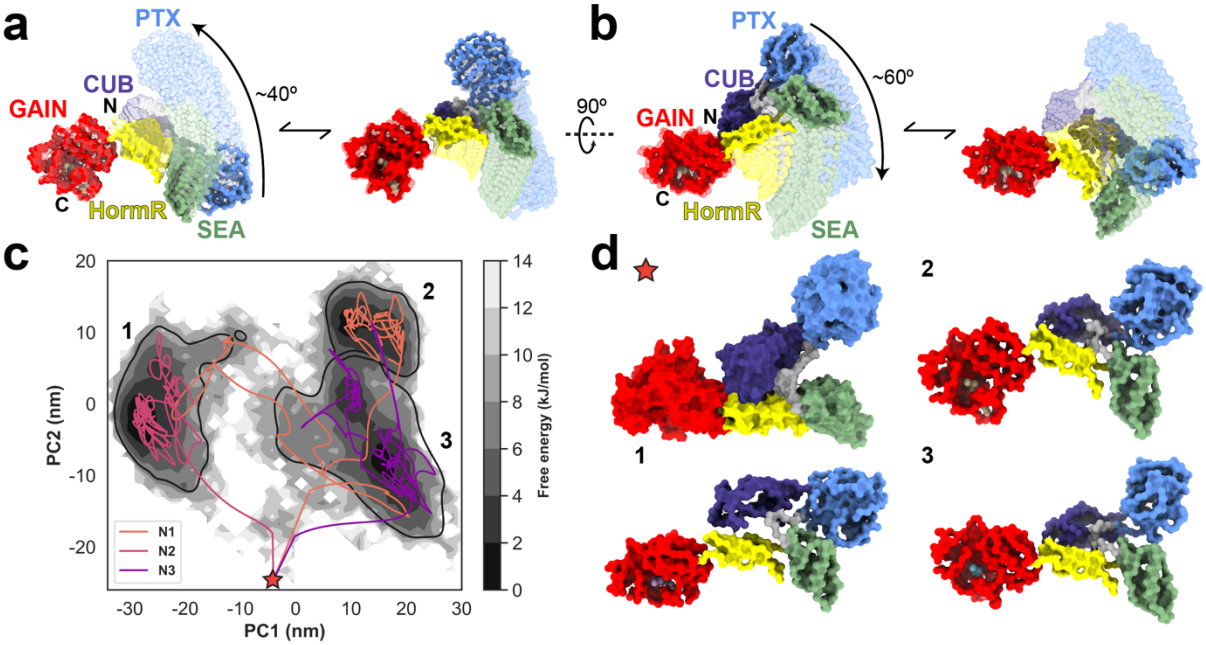

Fig. 3: Principal component analysis reveals multiple conformations of ADGRG6 –ss ECR with the CUB domain putative ligand binding site docked onto HormR. Principal component analysis was performed on the α–carbon coordinates of concatenated WT ADGRG6 –ss ECR simulations. **(a):** Projection of the α–carbons along PC1 shows a 40 º bend of the ECR about the GAIN domain. The initial (left) and final (right) frames of the projection are shown as opaque structures, and intermediates are displayed transparently. **(b):** Projection of the α–carbons along PC2 shows a 60 º bend of the ECR about the GAIN domain orthogonal to PC1. Shown as in (a). **(c):** Free energy surface calculated on the PC1–2 space with individual simulation trajectories overlaid as continuous lines. The red star represents the starting frame of the simulation. Black borders labeled 1–3 denote hierarchical clusters on this free energy surface. **(d):** The starting frame and the three centroids from panel (c) are shown as α–carbon surface representations to represent favored conformations across ADGRG6 –ss ECR simulation space.

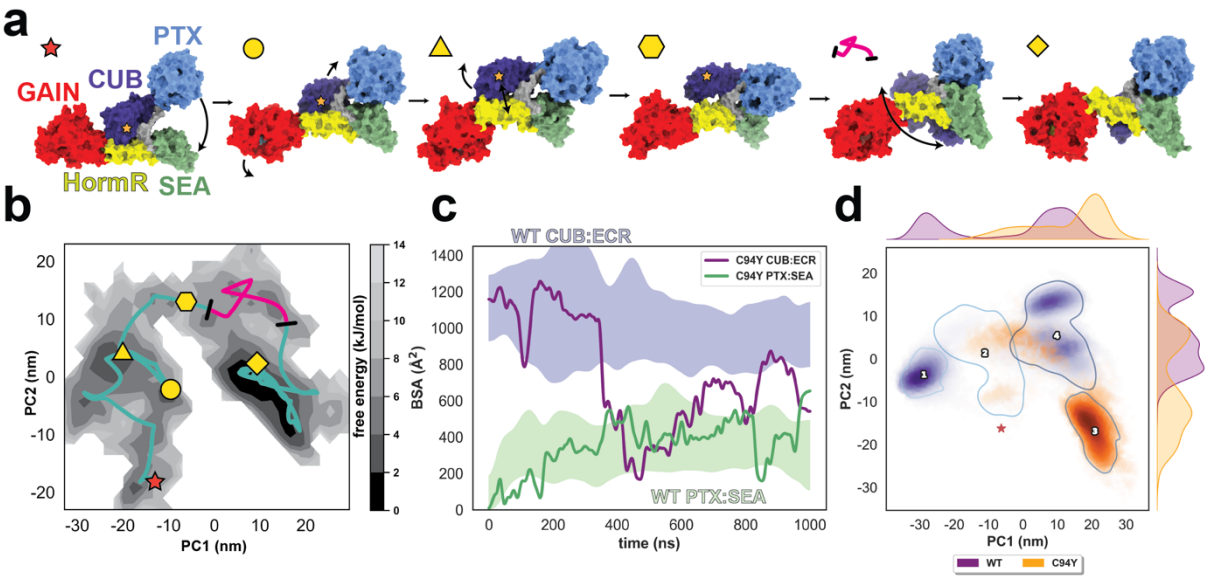

Fig. 4: The ADGRG6 –ss ECR mutant C94Y breaks the CUB:ECR interface and exposes the CUB ligand binding site. (a): Representative frames of C94Y –ss in MD show conformational transitions throughout the simulation. The starting point of the simulation is represented as a red star and the location of C94Y is marked by a gold star. PTX docks onto SEA (yellow circle), and then CUB dissociates from HormR (yellow triangle, then yellow hexagon). After CUB samples several conformations (magenta bounded line), it docks against the side of HormR with its ligand binding surface exposed (yellow diamond). **(b):** Free energy surface calculated on the PC1–2 space. A teal line indicates the C94Y simulation trajectory, with different shapes corresponding to the structures shown in panel A. **(c):** Buried surface area (BSA) of CUB:ECR and PTX:SEA interfaces over time. Dark lines represent the C94Y simulation, and the shaded intervals represent the bounds of the WT simulations for both interfaces. **(d):** Comparison of the WT (purple) and C94Y simulations (orange) in a combined essential space. Blue boundaries show hierarchical cluster boarders. 1D histograms represent density of projections of each simulation along each PC. The red star is a projection of the starting point of the simulation onto this PC space.

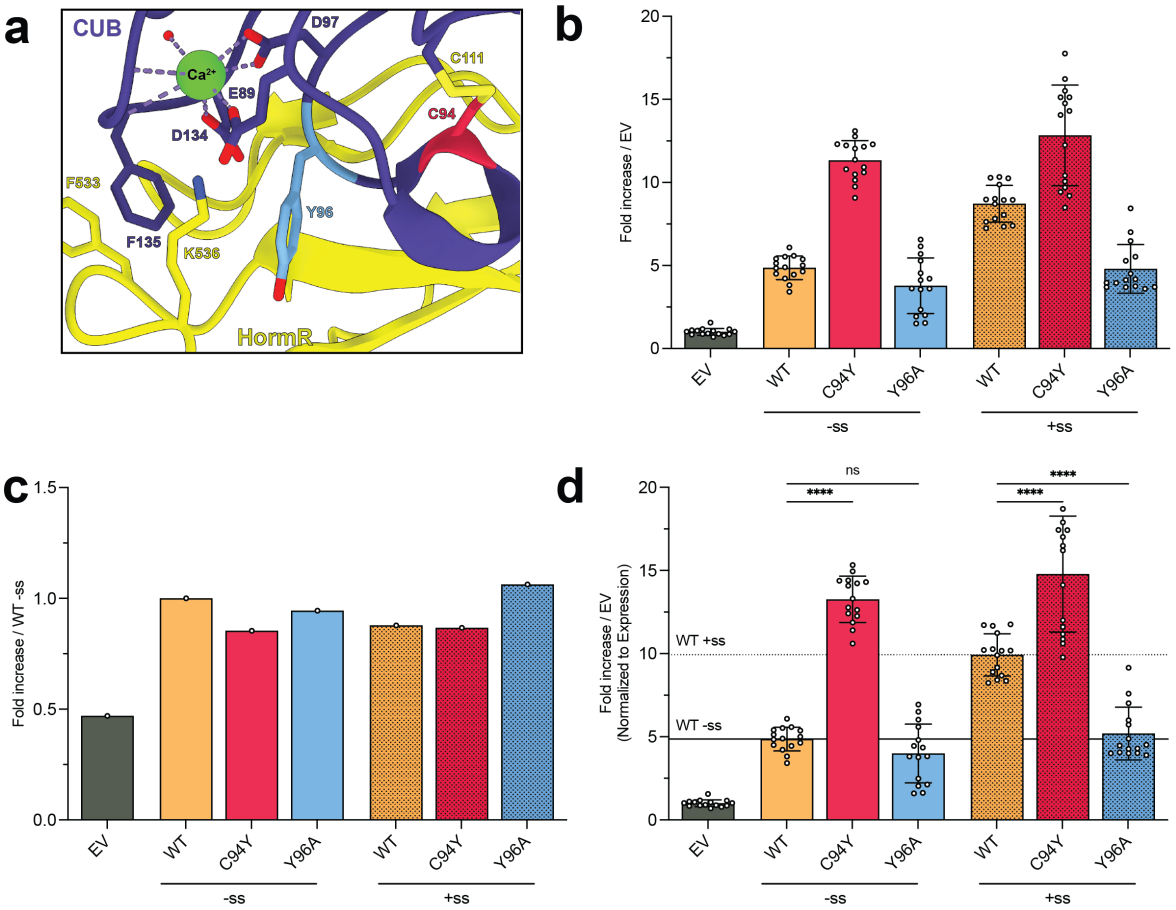

Fig. 5: Point mutants sourced from cancer patients modulate ADGRG6 cAMP signaling. (a): Close–up of the CUB/HormR interface from the crystal structure with key residues involved in the interaction shown as sticks. Residues which vary in cancer patients are colored differently (C94 magenta and Y96 light blue). The bound Ca^{2+} ion is shown as a green sphere with coordination shown as dotted lines. **(b):** Basal cAMP signaling of ADGRG6 constructs shown as fold change over empty vector (EV). Mutants are grouped by absence (–ss) or presence (+ss) of the ECR splice insert. **(c):** Relative cell surface expression levels for ADGRG6 constructs shown as fold change over WT –ss. See supplementary Fig. S4 for raw flow cytometry data. **(d):** Basal cAMP signaling represented as fold change over EV normalized to cell–surface expression with cancer mutants colored as in (a). Horizontal lines show the mean normalized signaling levels for WT constructs. **** – $p<0.0001$, ns – not significant; one–way ANOVA test with Tukey's correction for multiple comparisons. Each condition was compared to every other condition, but not all comparisons are shown for clarity. The following comparison (WT –ss vs. WT +ss) results in ****, $p<0.0001$ and (C94Y –ss vs. C94Y +ss) results in ns but these are not shown for clarity. N=3 independent experiments were performed with five replicates each.

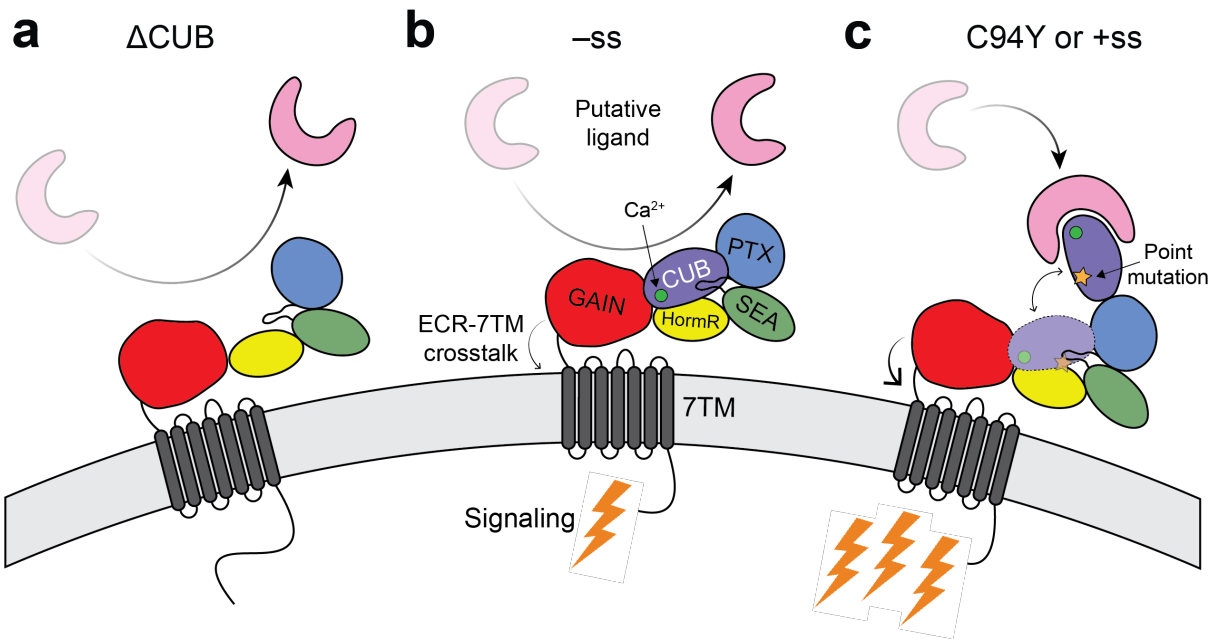

Fig. 6: Model for regulation of ADGRG6 signaling by its CUB domain. ADGRG6 is shown as a cartoon model with the putative ligand shown as a pink U–like shape and signaling shown as golden lightning bolts. A bound calcium ion is depicted as a green circle inside the CUB domain. The point mutation in the CUB domain is shown as a golden star. More lightning bolts indicate a higher level of signaling. **(a):** The ΔCUB receptor is unable to either bind the intramolecular HormR site or a putative extracellular ligand and has significantly decreased cAMP signaling (no lightning bolts). **(b):** For the ADGRG6 –ss receptor, the CUB/HormR interface remains intact. The –ss receptor signals modestly (one lightning bolt) and the CUB domain is unable to bind a putative extracellular ligand. **(c):** Mutants which break the CUB/HormR interface but not the canonical CUB ligand binding site displace the CUB domain from HormR. The receptor then accesses a higher signaling state (three lightning bolts) upon conformational change.

Supplementary Figures

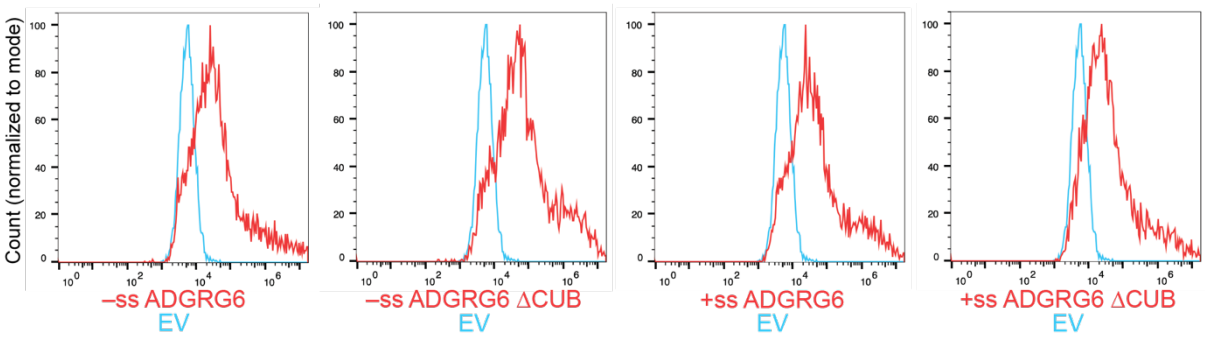

Supplementary Fig. S1: Expression levels for ADGRG6 ΔCUB constructs. Representative flow cytometry data showing expression levels of the N–terminally FLAG–tagged constructs used for cAMP signaling assays shown in Figure 1. These are measured using AlexaFluor–488 labeled α–FLAG antibodies. Each plot is overlaid with EV from the same experiment to highlight background labeling of cells. The cell count in the Y axis is normalized to the mode of each dataset.

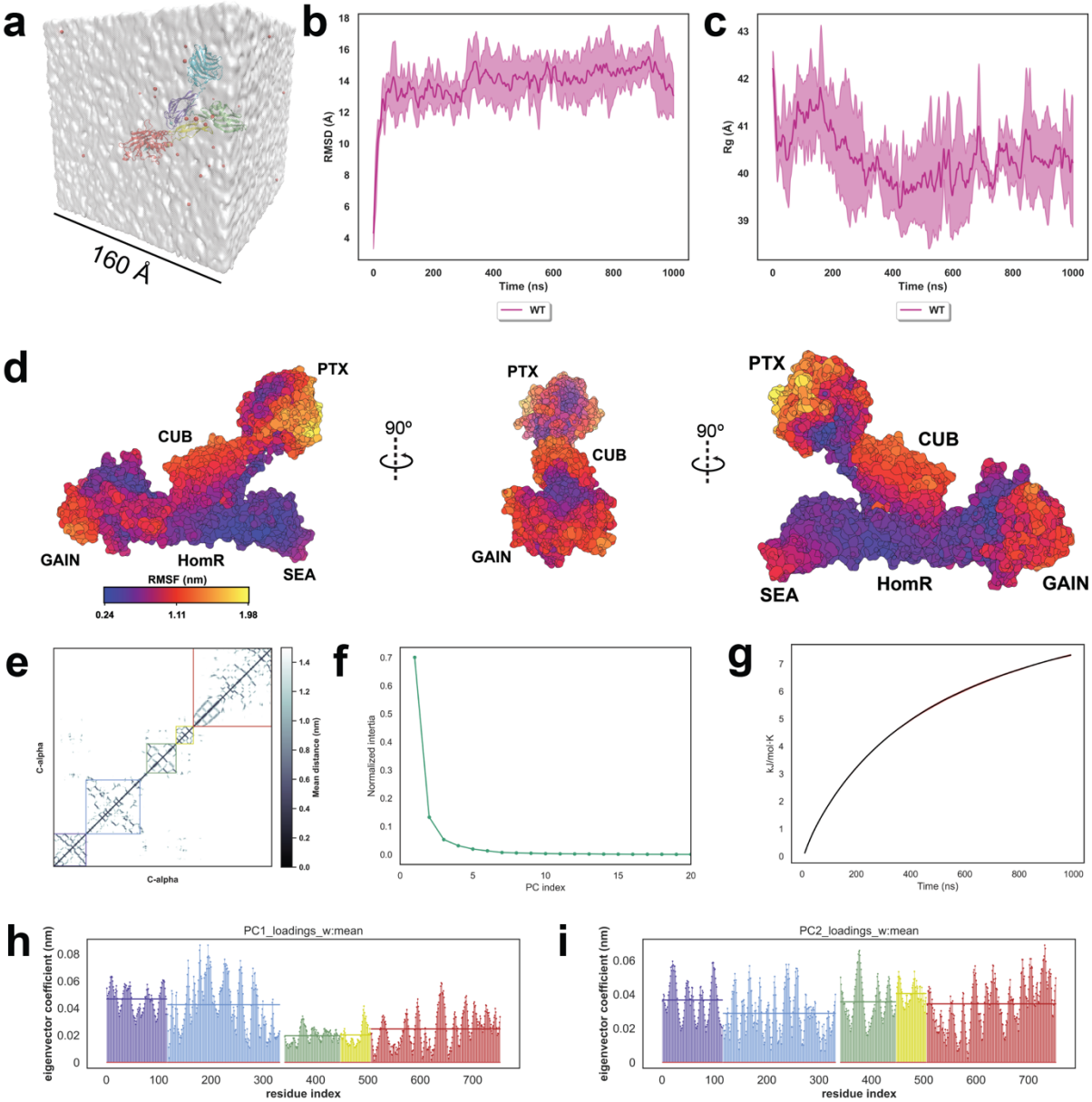

Supplementary Fig. S2: Dynamics of the WT zfADGRG6 –ss ECR throughout three one–microsecond MD simulations. (a): System simulated for each MD experiment, with cubic water box shown and sodium counterions shown as red spheres. **(b):** Mean Root–mean–square deviation (RMSD, dark line) and standard deviation (shaded region) of the Cα atoms from the crystal structure computed across the three simulations. **(c):** Radius of gyration (R_g) mean (dark line) and standard deviation (shaded region) across all three simulations. **(d):** Root–mean–square fluctuation (RMSF) from the average position for each residue mapped onto a surface representation of the zfADGRG6 –ss ECR crystal structure shown from three different views. **(e):** Mean distance matrix between each alpha carbon computed across all three simulations. Colored boxes denote domain boundaries, and data outside of colored boxes represent interdomain contacts. **(f):** Scree plot showing the variance of the concatenated WT simulations captured by each PC. The first 20 PCs are shown for clarity. **(g):** Cumulative entropy upper bound across all three simulations computed by Schlitter's formula. Black line denotes mean and red boundaries denote the standard deviation. **(h):** Magnitude of the Cartesian components for each Cα in PC1 colored by domain to represent the conformational variance of each domain. Colored horizontal lines denote mean magnitudes for each domain. **(i):** Magnitude of the Cartesian components for each Cα in PC2 represented as in (h).

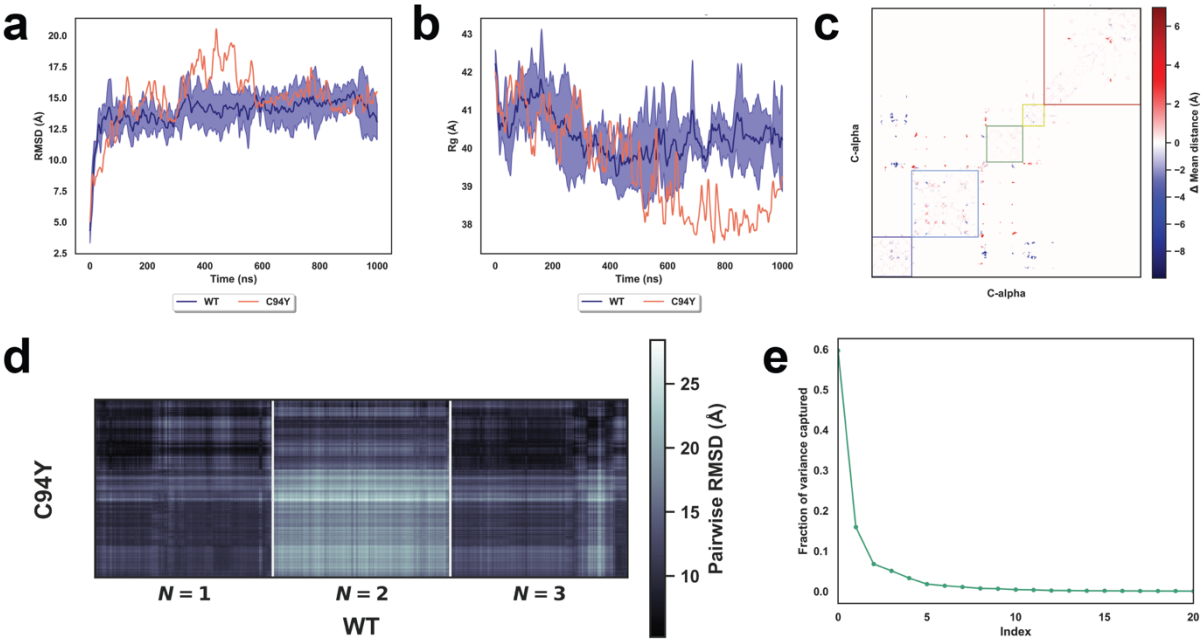

Supplementary Fig. S3: Dynamics of the ADGRG6 –ss ECR C94Y simulation. (a): Cα RMSD of the C94Y simulation (orange) compared to the WT simulations (purple line and shaded region = mean ± standard deviation). **(b):** R_g comparison between the C94Y and WT simulations. **(c):** Cα–Cα contact comparison between the WT and C94Y simulations. Negative values (blue) represent a greater distance in C94Y than WT, and positive values (red) represent a closer distance in C94Y than WT. **(d):** Cα RMSDs between every structure in the C94Y simulation and WT simulations. **(e):** Scree plot showing the variance of the C94Y simulation captured by each PC. The first 20 PCs are shown for clarity.

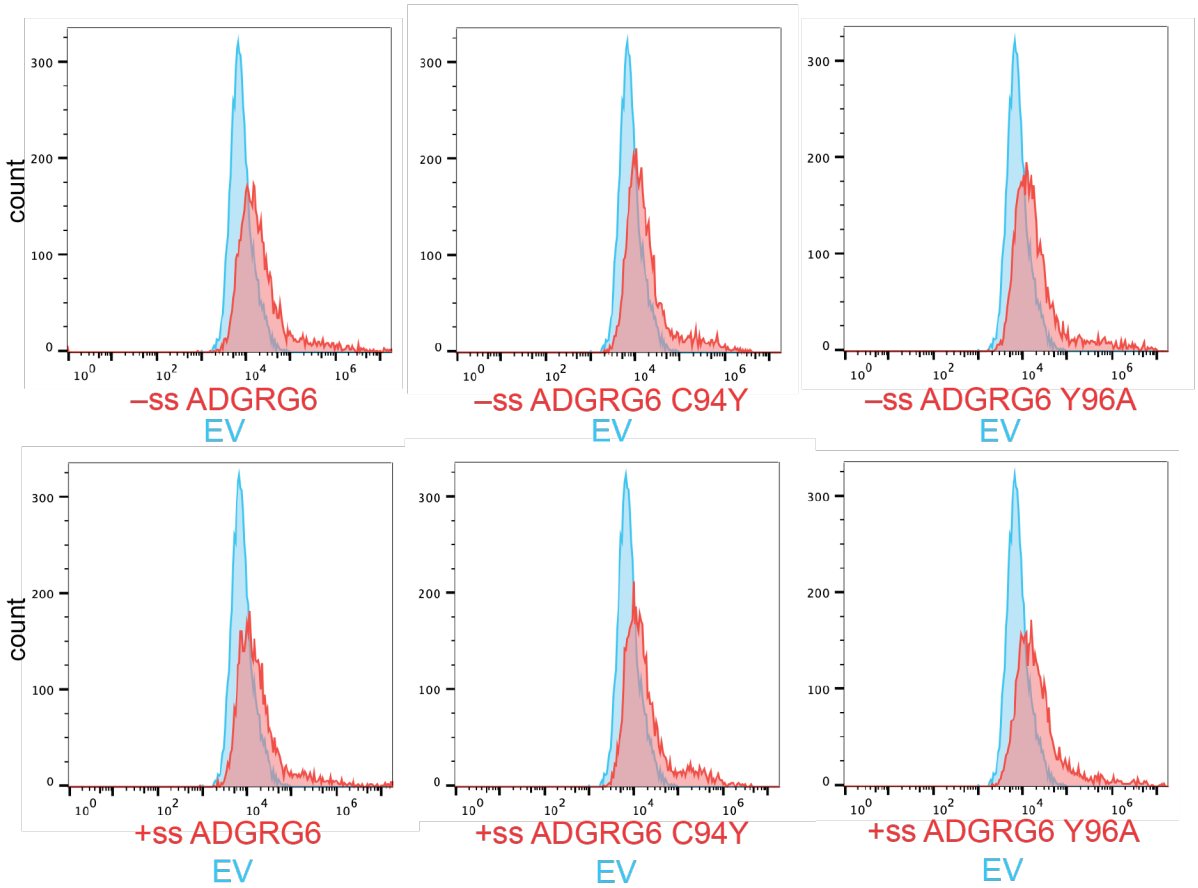

Supplementary Fig. S4: Expression levels for ADGRG6 and cancer mutants. Flow cytometry data showing expression levels of the N–terminally FLAG–tagged constructs used for cAMP signaling assays in Figure 5. These are measured using AlexaFluor–488 labeled α–FLAG antibodies. Each plot is overlaid with EV from the same experiment to show background labeling of cells.

Supplementary Videos

Supplementary Video SV1: A full microsecond simulation of the WT zfADGRG6 –ss ECR smoothed by a low–pass filter for visualization. Domains are colored according to the scheme in Fig. 1A–B and atoms are represented in a surface view.

Supplementary Video SV2: Projection of the zfADGRG6 –ss ECR α–carbons along the first principal component (PC1) obtained from PCA on the concatenated WT simulations. Cα atoms are shown in a surface view.

Supplementary Video SV3: Projection of the zfADGRG6 –ss ECR α–carbons along the second principal component (PC2) obtained from PCA on the concatenated WT simulations. Cα atoms are shown in a surface view.

Supplementary Video SV4: A microsecond simulation of the C94Y zfADGRG6 –ss ECR smoothed by a low–pass filter for visualization. Domains are colored according to the scheme in Fig. 1A–B and atoms are represented in a surface view.

Supplementary Video SV5: Projection of the zfADGRG6 –ss ECR α–carbons along the first principal component (PC1) obtained from PCA on the C94Y simulation. Cα atoms are shown in a surface view.

Supplementary Video SV6: Projection of the zfADGRG6 –ss ECR α–carbons along the second principal component (PC2) obtained from PCA on the C94Y simulation. Cα atoms are shown in a surface view.